Chapter

Simulation on the Surface Charge Behaviors of Epoxy Insulator by Corona Discharge

Boxue Du, Hucheng Liang and Jin Li

Abstract

A majority of the high voltage (HV) electrical equipment which has solid-gas insulation has suffered greatly from the accumulation of the surface charges generated from the corona discharge. The local electric field may be distorted by the surface charge's existence and in turn causes the surface flashover faults in excessive circumstances. Consequently, it's significant to work out the mechanism of the procedure of the surface charge accumulation. A simulation model which combines both the charge trapping-detrapping procedure and the plasma hydrodynamics was created. The outcome of the simulation has agreed with the experimental results. The corona discharge intensity rises in the initial stage and then reduces as time goes by. There are various shapes of the surface potential distribution curves at various times. The central value increases quickly with time first and at last becomes saturated. Surface charges are observed in the epoxy insulator's skin layer, some of them are mobile but some are captured by traps.

Keywords: DC power transmission, epoxy insulator, corona discharge, FEM simulation, surface charge, trapping and detrapping

1. Introduction

A majority of the electrical equipment which has solid-gas insulation has suffered seriously from the existence of surface charges. Electrons and/or ions generated by the corona discharge migrate under electric force and accumulate on the insulator surface. In some cases, this may cause the local electric field distortion and even the surface flashover faults [1–3]. The surface charge distribution of GIS (gas insulated switchgear) spacer was presented in Ref. [4], which concluded that the distribution of surface charge always reaches its steady state after some time. Ref. [5] measured the surface potential decay (SPD) process of epoxy resin and found that this process takes several hours. Ref. [6] used the fluorination treatment to enhance the SPD rate of epoxy resin. Ref. [7] discussed the surface charge behaviors after various pulse application. In addition, several scholars have established the drift-diffusion equations for the purpose of describing the charge trapping-detrapping procedure within the bulk of the insulator [8–12]. Moreover, the plasma hydrodynamics models are adopted widely for the purpose of simulating the gas discharge procedure [13–16]. Nevertheless, very few people have ever tried to

combine the charge trapping-detrapping procedure and the plasma hydrodynamics to simulate the surface charge accumulation procedure.

This chapter presents a needle-plane model for the purpose of studying the surface charge accumulation procedure. It is the first time that the charge trapping-detrapping procedure combines with the plasma hydrodynamics. Compared with the existing simulation models for surface charge accumulation, our model has some advantages: (1) in the ionization region, the existing models used some simplified charge transport equations to simulated the generation and transport process of charged ions. Our model is closer to the reality with many physicochemical reactions (the collision ionization etc.) in consideration; (2) in the insulator bulk, the charge trapping-detrapping process is taken into consideration; (3) in our model, the charge transport parameters (carrier mobility, carrier diffusion coefficient etc.) are obtained from solving the Boltzmann equation, which is more reliable. This chapter aims at doing some fundamental researches on the procedure of the surface charge accumulation rather than guiding the engineering application. The needle-plane model has usually been adopted to do the SPD test in many published research papers, which is of great convenience for us to compare between the outcomes of experiment and simulation. This chapter may provide some help for readers to understand the surface charge accumulation process through some simulated details which is difficult to be gained from the experimental measurements.

2. Simulation model

2.1 Geometric model

According to **Figure 1**, the needle-plane electrode system's schematic diagram is considered to be axisymmetric and therefore, it is simplified to a 2D issue. Within a lot of papers, the model often added with a mesh electrode was adopted for charging the insulators for the purpose of doing surface charge measurements. The needle electrode's radius curvature is set to 50 μm in this chapter. The grounded (GND) electrode is placed which has a thickness of 0.5 mm and a radius of 20 mm. The axial distance between the insulator upper face and the needle tip is 3.5 mm.

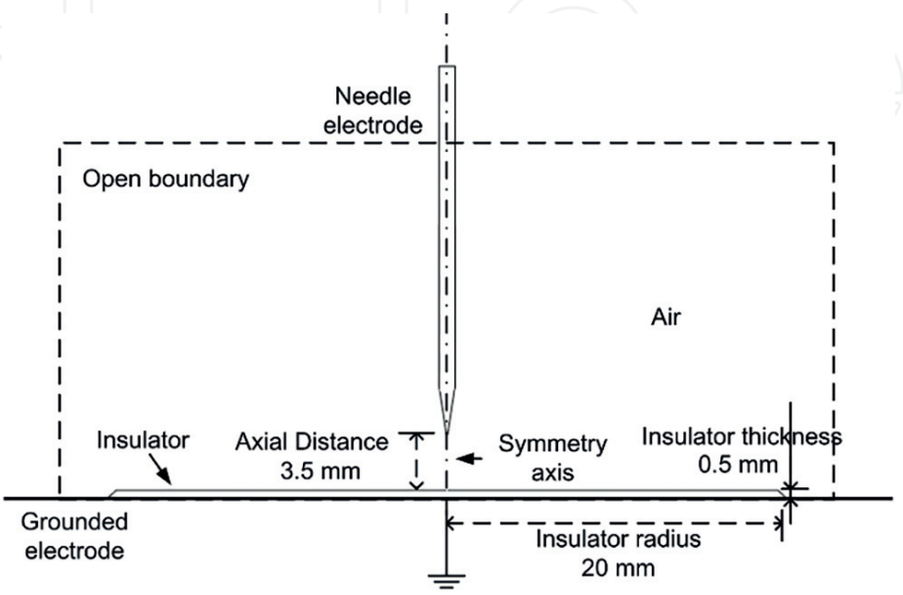

Figure 1.
A schematic diagram of the needle-plane electrode system.

2.2 Corona discharge in air

On the basis of the needle-plane model shown before, the corona discharge process is going to be simulated in this section.

The governing equations for the drift-diffusion of the electron energy density n and the electron density n_e are presented below:

$$\frac{\partial}{\partial t}(n_e)+\nabla\cdot[-n_e(\mu_e\cdot\vec{E})-D_e\cdot\nabla n_e]=R_e \tag{1}$$

$$\frac{\partial}{\partial t}(n_\varepsilon)+\nabla\cdot[-n_\varepsilon(\mu_\varepsilon\cdot\vec{E})-D_\varepsilon\cdot\nabla n_\varepsilon]+E\cdot\Gamma_e=R_\varepsilon \tag{2}$$

where the energy mobility μ_ε, the electron mobility μ_e, the energy diffusivity D_ε, and the electron diffusivity D_e are computed through working out the two-term Boltzmann equation. R_ε and R_e are the energy loss and electron source because of inelastic collisions. In this simulation, *M-N* three-body reactions and *N* two-body reactions are taken into consideration,

$$R_e=\sum_{j=1}^{N}x_jk_jN_nn_e\Delta n_{ej}+\sum_{j=N+1}^{M}x_{j1}x_{j2}k_jN_n{}^2n_e\Delta n_{ej} \tag{3}$$

$$R_\varepsilon=\sum_{j=1}^{P}x_jk_jN_nn_e\Delta\varepsilon_j \tag{4}$$

$$N_n=pT/k_B \tag{5}$$

where x_{j2} x_{j1} and x_j, are the species' mole fractions which are involved in reaction j; $\Delta\varepsilon_j$ and Δn_{ej} are the energy loss (V) and electron increment of reaction j, respectively; p is the atmospheric pressure of air (1 atm); N_n is the total neutral density ($1/m^3$); and k_j is the rate coefficient of reaction j (m^3/s or m^6/s), which is able to be gained through working out the two-term Boltzmann equation as well.

$$\varepsilon=\frac{n_\varepsilon}{n_e}=\frac{3}{2}T_e \tag{6}$$

where ε and T_e is the mean electron energy (V) and the electron temperature (V), respectively.

In terms of heavy species, every species' mass fraction is able to be gained through working out the equations below,

$$\rho\frac{\partial}{\partial t}(w_k)-\nabla\cdot\vec{j}_k=R_k \tag{7}$$

$$\vec{j}_k=\rho w_k\vec{V}_k \tag{8}$$

$$\vec{V}_k=D_k(\nabla w_k/w_k+\nabla M_n/M_n)-z_k\mu_k\vec{E} \tag{9}$$

where E is E-field strength (V/m); μ_k is averaged mobility of species k ($m^2/(V\,s)$); z_k is charge number of species k; M_n is s mean molar of air (kg/mol); D_k is averaged diffusion coefficient of species k (m^2/s); R_k is generation rate of species

k (kg/(m^3·s)); j_k is flux of species k; w_k is the mass fraction of species k; ρ is density of air (kg/m^3). In this simulation, M-N three-body reactions and N two-body reactions that change the species k's mass fraction are taken into consideration,

$$R_k = \frac{M_k}{N_A}\left(\sum_{j=1}^{N} k_j x_{j1} x_{j2} N_n^{\,2} \Delta n_{kj} + \sum_{j=N+1}^{M} k_j x_{j1} x_{j2} x_{j3} N_n^{\,3} \Delta n_{kj}\right) \tag{10}$$

$$x_k = \frac{M_n w_k}{M_k} \tag{11}$$

where x_{j3}, x_{j2} and x_{j1} are the species' mole fractions which are involved in reaction j; M_k is species k's molar mass (kg/mol); Δn_{kj} is species k increment of reaction j; N_A is Avogadro constant. Eq. (10) presents the relation between species k's mass fraction and the mole fraction.

Eq. (12) is the definition of the mixture averaged diffusion coefficient D_k while Eq. (13) is the definition of the mixture averaged mobility μ_k in accordance with the Relation of Einstein,

$$D_k = \frac{1 - w_k}{\sum_{j \neq k}^{Q} x_j / D_{k,j}} \tag{12}$$

$$\mu_k = \frac{eD_k}{k_B T} \tag{13}$$

where T is gas temperature (K); k_B is constant (J/K) of Boltzmann; e is unit charge (C); $D_{k,j}$ is the binary diffusion coefficient between species k and j, which is able to be evaluated through the Fuller Formula,

$$D_{k,j} = \frac{0.0101 T^{1.75} \sqrt{\frac{1}{M_k} + \frac{1}{M_j}}}{P\left[\left(\sum v_k\right)^{1/3} + \sum v_j\right)^{1/3}]^2} \tag{14}$$

where $\sum v_j$ and $\sum v_k$ is the species k and j's diffusion volume (cm^3/mol); M_j and M_k are species k and j's molar mass (kg/mol).

The boundary conditions on the surface of insulator and electrodes are defined as,

$$\vec{n} \cdot \vec{\Gamma}_e = \frac{1}{4} v_{e,th} n_e - \sum_p \gamma_p (\vec{\Gamma}_p \cdot \vec{n}) \tag{15}$$

$$\vec{n} \cdot \vec{\Gamma}_\varepsilon = \frac{5}{12} v_{e,th} n_\varepsilon - \sum_p \varepsilon_p \gamma_p (\vec{\Gamma}_p \cdot \vec{n}) \tag{16}$$

$$v_{e,th} = \left(\frac{8 k_B T_e}{\pi m_e}\right)^{1/2} \tag{17}$$

$$\vec{n} \cdot \vec{j}_k = \frac{1}{4} v_{k,th} \rho w_k + \alpha \rho w_k z_k \mu_k (\vec{E} \cdot \vec{n}) \tag{18}$$

$$v_{k,th} = \left(\frac{8k_B T}{\pi m_k}\right)^{1/2} \tag{19}$$

where γ_p is the secondary emission coefficient; ε_p is the secondary electrons' mean energy (V); $\alpha \cdot z_k/|z_k| = 1$ if electric field can be directed towards the boundary; $\alpha \cdot z_k/|z_k| = 0$ if electric field can be directed away from the boundary; T is regarded as the environment temperature (K) and $v_{k,th}$ is the species k 's thermal velocity (m/s).

The definitions of the boundary conditions at the open boundary are as follows:

$$\vec{n} \cdot \nabla n_e = 0 \tag{20}$$

$$\vec{n} \cdot \nabla n_\varepsilon = 0 \tag{21}$$

$$\vec{n} \cdot \nabla w_k = 0 \tag{22}$$

Ions may become neutral species because of the surface reactions. Just several typical surface reactions will be considered for simplification in the paper.

$$N_2^+ \rightarrow N_2 \qquad O_2^+ \rightarrow O_2$$

$$O_2^- \rightarrow O_2 \qquad O_4^+ \rightarrow 2O_2$$

The plasma hydrodynamics model is made up of 19 reactions and 10 species (e.g.: O_4^+, O, O_3, O_2^-, O_2^+, N_2, N_2, O_2, N_2^+, O_2^+). Some particular physicochemical reactions are listed in **Table 1** which are considered in the model after some reduction. These collision reactions' energy losses and cross sections are extracted from

No.	Formula	Type	$\Delta\varepsilon$ (eV)	Δn_e	Rate coefficient
1	$N_2 + e \rightarrow e + N_2$	Elastic	0	0	—
2	$O_2 + e \rightarrow e + O_2$	Elastic	0	0	—
3	$N_2 + e \rightarrow 2e + N_2^+$	Ionization	−15.6	1	—
4	$O_2 + e \rightarrow 2e + O_2^+$	Ionization	−12.06	1	—
5	$N_2 + e \rightarrow e + N_2$	Excitation	−8	0	—
6	$O_2 + e \rightarrow e + O_2$	Excitation	−5.5	0	—
7	$O_2^+ + O_2 + M \rightarrow O_4^+ + M$	Reaction	—	—	$2.04 \times 10^{-34}\, T^{-3.2}$
8	$O_4^+ + e \rightarrow 2O_2$	Reaction	—	−1	$1.4 \times 10^{-12}\, (300/T_e)^{0.5}$
9	$O_2^+ + e \rightarrow 2O$	Reaction	—	−1	$2.42 \times 10^{-13}\, (300/T_e)$
10	$2O_2 + e \rightarrow O_2 + O_2^-$	Reaction	—	−1	$2 \times 10^{-41}\, (300/T_e)$
11	$O_4^+ + O_2^- \rightarrow 3O_2$	Reaction	—	—	1×10^{-13}
12–13	$O_4^+ + O_2^- + M \rightarrow 3O_2 + M$	Reaction	—	—	2×10^{-37}
14–15	$O_2^+ + O_2^- + M \rightarrow 2O_2 + M$	Reaction	—	—	2×10^{-37}
16–17	$O + O_2 + M \rightarrow O_3 + M$	Reaction	—	—	2.5×10^{-46}
18	$e + N_2^+ + N_2 \rightarrow 2N_2$	Reaction	—	−1	$6.07 \times 10^{-34} T_e^{-2.5}$
19	$2e + N_2^+ \rightarrow N_2 + e$	Reaction	—	−1	$5.65 \times 10^{-27} T_e^{-0.8}$

Units: $m^3\, s^{-1}$ for two-body reactions, $m^6\, s^{-1}$ for three-body reactions, K for T_e and T; Notes: M = O_2, N_2.

Table 1.
Some typical physicochemical reactions in the corona discharge model.

papers [17, 18]. The initial electron density is set to 1×10^9 1/m^3 and the O_2 to N_2 ratio is 1:4. Δn_e means the electron increment of each reaction.

2.3 Detrapping process and charge trapping in the epoxy insulator

Electrons are going to be injected into the discharge channel when it reaches the surface of the insulator. The positive ions are converted into the neutral particles through the reactions on the surface. It can be assumed that we can also inject some holes into the insulator. Both the holes and the electrons are possible to be released from traps through thermal excitation and captured by traps when transporting. It should be noticed that the conduction on the surface is not considered in this chapter because very little tangential component exists in the electric field distribution along the surface of the insulator.

$$\frac{\partial n_{mb}}{\partial t} + \nabla \cdot \vec{J}_c^e = n_{tr} P_{de} - n_{mb} P_{tr} - R_1 n_{mb} h_{tr} - \frac{1}{\tau} \Delta n \tag{23}$$

$$\frac{\partial n_{tr}}{\partial t} = n_{mb} P_{tr} - R_2 n_{tr} h_{tr} - R_3 n_{tr} h_{mb} \tag{24}$$

$$\vec{J}_c^e = \mu_e n_{mb} \cdot \nabla V - D_e \cdot \nabla n_{mb} \tag{25}$$

$$\frac{\partial h_{mb}}{\partial t} + \nabla \cdot \vec{J}_c^h = h_{tr} P_{de} - h_{mb} P_{tr} - R_3 n_{tr} h_{mb} - \frac{1}{\tau} \Delta h \tag{26}$$

$$\frac{\partial h_{tr}}{\partial t} = h_{mb} P_{tr} - R_1 n_{mb} h_{tr} - R_2 n_{tr} h_{tr} \tag{27}$$

$$\vec{J}_c^h = -\mu_h h_{mb} \cdot \nabla V - D_h \cdot \nabla h_{mb} \tag{28}$$

where τ is the non-equilibrium carriers' lifetime (s); R_3, R_2 and R_1 are the recombination coefficients (m^3/s); P_{de} and P_{tr} are the detrapping and trapping probability of hole and electron (1/s); n_{mb} is the mobile electron density (1/m^3); μ_h and μ_e are the hole and electron's diffusion coefficient (m^2/s); V is potential (V); n_{tr} is the trapped electron density (1/m^3); J_c^h and J_c^e are the mobile electron and hole's flux (1/(m^2 s)); h_{tr} is trapped hole density (1/m^3); h_{mb} is the mobile hole density (1/m^3).

Inspired by the theories in the semiconductor physics on the non-equilibrium, the products of the hole density h_0 and mobile electron density are considered to be constants in the insulator within the condition of the thermal equilibrium.

q

$$n_0 h_0 = N_v N_c e^{-E_g / k_B T} \tag{29}$$

where E_g is the insulator's energy gap (eV); N_c and N_v are states' effective densities at conduction band bottom and the valence band top (1/m^3). Supposing the hole density and electron are h_{mb} and n_{mb} in an unbalanced condition, Δh and Δn is able to be obtained through working out Eq. (29). The procedure of the electron–hole recombination is represented by positive Δh and Δn while the electron-hole pairs' generation is represented by negative Δh and Δn.

$$n_0 h_0 = (n_{mb} - \Delta n)(h_{mb} - \Delta h) \tag{30}$$

$$\Delta n = \Delta h = \frac{(n_{mb} + h_{mb}) - \sqrt{(n_{mb} - h_{mb})^2 + 4n_0 h_o}}{2} \tag{31}$$

We can describe the boundary conditions at the insulator's upper surface as follows:

$$-\vec{n} \cdot \vec{\Gamma}_{n_{mb}} = \vec{n} \cdot \vec{j}_e \tag{32}$$

$$-\vec{n} \cdot \vec{\Gamma}_{h_{mb}} = \vec{n} \cdot \vec{j}_i \tag{33}$$

where j_i and j_e are ion and electron flux through insulator's upper surface in corona discharge model (1/m^2 s).

We can describe the boundary conditions at the insulator's lower surface as follows:

$$\vec{n} \cdot \vec{\Gamma}_{n_{mb}} = \vec{n} \cdot (-\mu_e n_{mb} \cdot \nabla V) \tag{34}$$

$$\vec{n} \cdot \vec{\Gamma}_{h_{mb}} = \vec{n} \cdot (-\mu_h h_{mb} \cdot \nabla V) \tag{35}$$

Some of the epoxy's parameters adopted in the charge trapping-detrapping model are listed in **Table 2**. Among them, some referred to papers and some were gained from experimental measurements [12, 19, 20].

2.4 Poisson equation

The p species (negative ions, positive ions and electrons) are made up by the corona discharge model and z_k is the species k's charged number. Therefore, we can describe the Poisson equation in the air as follows:

$$-\nabla^2 V = e(\sum_{1}^{p} n_k z_k) / \varepsilon_0 \tag{36}$$

Parameters	Value
Charge carrier mobility (m^2/(V s))	
μ_e	1.0×10^{-14}
μ_h	1.0×10^{-14}
Charge carrier diffusion coefficient (m^2/s)	
D_e	2.6×10^{-16}
D_h	2.6×10^{-16}
Trapping and detrapping coefficients (1/s)	
P_{tr}	7.0×10^{-3}
P_{de}	7.7×10^{-5}
Recombination coefficients (m^3/s)	
R_1	8.0×10^{-19}
R_2	8.0×10^{-19}
R_3	8.0×10^{-19}

Table 2.
Some parameters of epoxy in the trapping-detrapping model.

where species k's density is n_k (1/m^3).

We can describe Poisson equation within insulator as follows:

$$-\nabla^2 V = e(h_{mb} + h_{tr} - n_{mb} - n_{tr}) / (\varepsilon_0 \varepsilon_r) \tag{37}$$

where ε_r is the insulator's relative dielectric constant.

We add a resistor R_b for the purpose of limiting the discharge current I_p. The definition of the voltage on HV electrode is as follows:

$$V = V_0 - I_p R_b \tag{38}$$

$$I_p = -\int (\vec{n} \cdot \vec{j}_i + \vec{n} \cdot \vec{j}_e) dS \tag{39}$$

where V_0 is the voltage of power supply (V); I_p is the discharge current (A), which can be obtained by integrating the current density on the boundary of the HV electrode; V is the potential on needle electrode (V).

The open boundary is as follows:

$$\vec{n} \cdot \nabla V = 0 \tag{40}$$

2.5. Surface potential measurement

Some surface potential measurement tests are implemented for the purpose of verifying this simulation's validity. The measurement system of the needle-plane electrode surface potential is shown in **Figure 2**. The HV electrode was put 3.5 mm over the central insulator and supplied HVDC voltages on it through a power source with high voltage. Needle electrode's radius curvature was ~50 μm. The design of the insulator was like a disc of 0.5 mm thick. The insulator was slid to the position 3 mm on a rail below the probe after charging for a minute, which was adopted for measuring the distribution of the surface potential. It is not difficult to obtain the distribution of the surface potential along the radial distance through the measurement of 5 points' values from the center to the insulator's edge.

3. Results and discussion

With DC −5 kV applied on the needle, the electric potential and force line distribution are simulated and presented in **Figure 3**. The electric potential's variation is represented by the gradient color which is presented in the color legend on

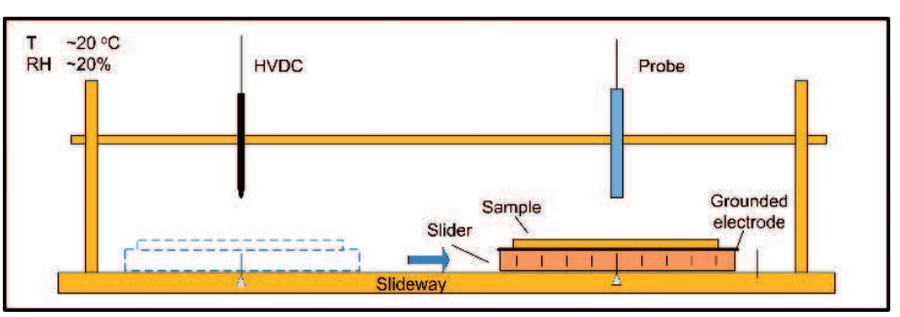

Figure 2.
A schematic diagram of the surface potential measurement system.

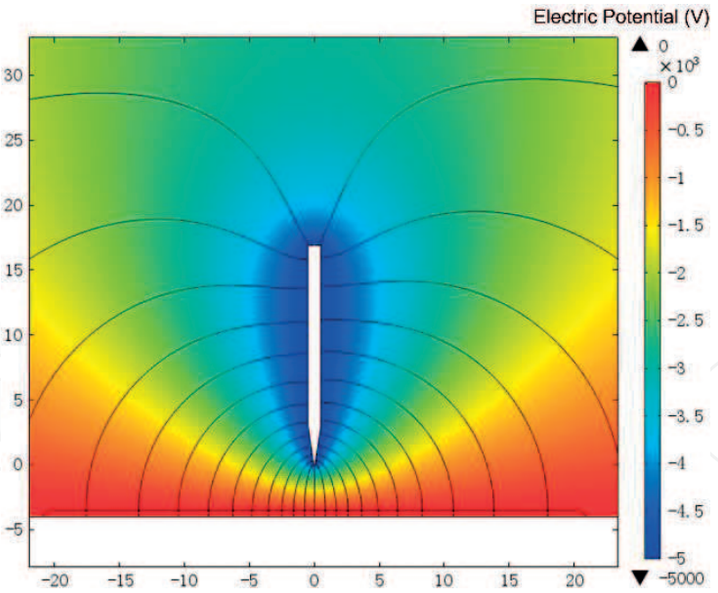

Figure 3.
The simulated distribution of electric potential and force lines.

the figure's right side. The electric force line distribution can be obtained through the calculation of the potential gradient. It can be seen that all the force lines go from the needle to the ground and stronger field strength at the needle tip is indicated by denser force lines. Consequently, the corona discharge is produced like an avalanche. Electrons with negative charge transport from the needle tip to the insulator's upper surface under electric force but ions with positive charge go oppositely, which causes the negative charges to accumulate on surface of insulator. In addition, very little tangential component of E-field exists on the surface of the insulator. Therefore, this chapter will not consider about the surface conduction.

Electron density's variation is shown in **Figure 4**. The electron density's variation is represented by the gradient color which is presented in the color legend on figures' right side. Here the E-field strength is high enough to produce electron-ion pairs and ionize the air due to the needle tip's small curvature radius. According to **Figure 4**, it can be seen that the electron avalanche's small crescent appears near the needle tip. Electrons gain higher speed from the needle tip under electric force, which produces more electrons through impact ionizations. We can see in **Figure 5b** that a clear increment exists in the electron avalanche's density and size. The electron avalanche's size becomes larger and larger at the time of moving to the insulator surface. The electron density's distribution can be shown in **Figure 4c**. The electron avalanche's head has reached the surface of the insulator at that time, which forms a clear discharge channel. Many electrons start accumulating on the surface of the insulator, which causes the E-field strength's disadvantages and the surface potential's rise. The discharge channel is barely able to be recognized from **Figure 4d**, which indicates the end of the corona discharge and surface charge accumulation.

According to **Figure 5**, the ion and electron densities are shown along the symmetry axis, which echoes **Figure 4** which is presented before. The axial coordinate $z = -3.5$ mm is the insulator surface and $z = 0$ mm is the needle tip. **Figure 5a** shows that the corona discharge is started from the needle tip. Positive charges concentrate at the tail and negative charges concentrate at the electron avalanche's head. Electrons are accelerated away with time, which produces more ions and electrons. **Figure 5b** shows that the peaks of the ion and electron densities have reached approximately 1×10^{15} 1/m^3. It is clear that the electron avalanche grows

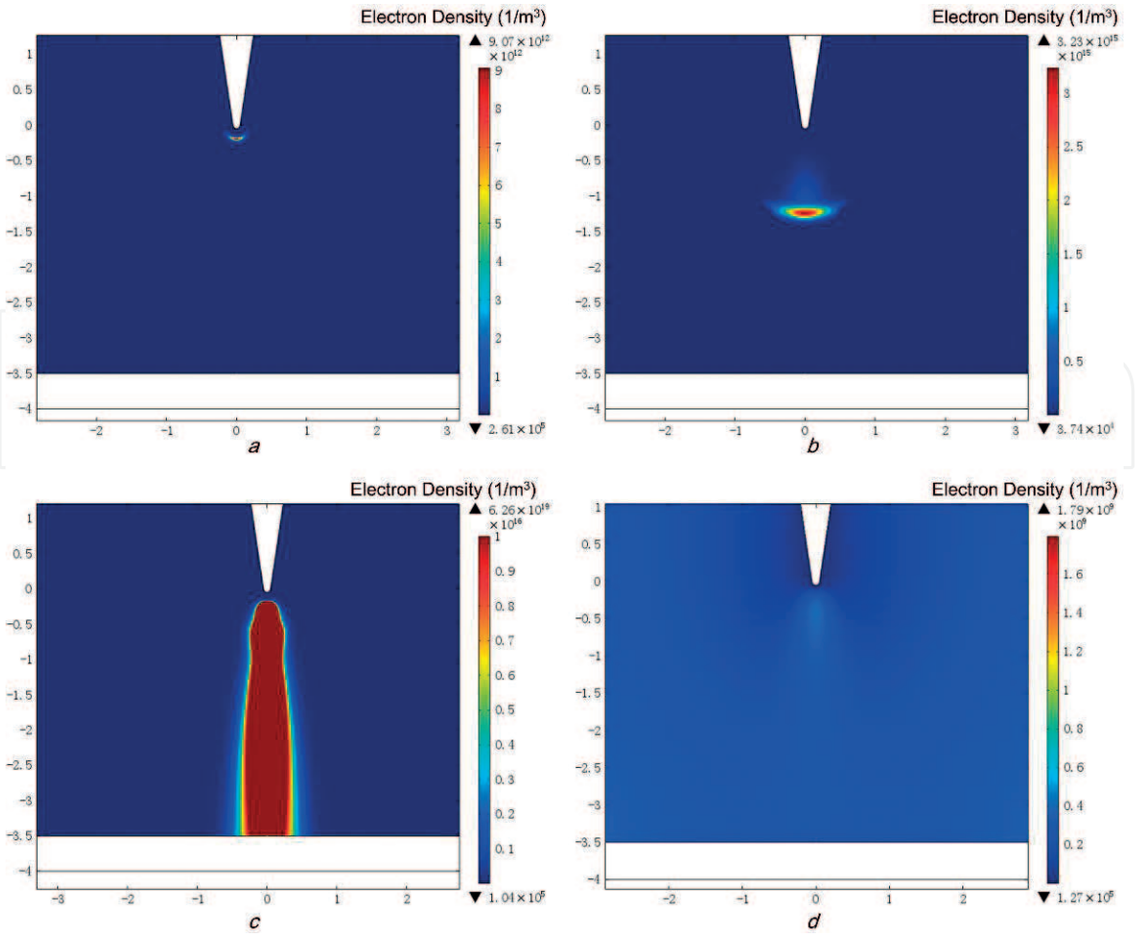

Figure 4.
The variation of electron density with the development of corona discharge: (a) 1 × 10⁻⁹ s, (b) 1.8 × 10⁻⁸ s, (c) 4.6 × 10⁻⁷ s, (d) 60 s.

sharply. The mobility of ions is much smaller than that of electrons. Therefore, they seldom move under electric force which results in the electron avalanche tail's extension. **Figure 5c** shows that the electron avalanche has reached the surface of the insulator for the purpose of forming a discharge channel. Both the ion and electron densities are increased by more than magnitude's four orders. Many negative charges have been accumulated as the discharge time goes by, which causes the field strength's disadvantages and increases the surface potential. The procedure of the corona discharge becomes weak. Thus, both the ion and electron densities reduces with time, which is presented in **Figure 5d**.

According to **Figure 6a**, the surface potential distributions are shown with the corona discharge's development. More electrons are able to be accumulated on the center of the surface because the needle electrode is above the center of the insulator directly. The peak of the surface potential appears in the central part and decreases to the edge from the central part. Additionally, the surface potential distributions' curves have various kinds of shapes at various times. The surface potential is ~2000 V at the center when time t = 1 s, which is much higher compared with that at the edge. One second is not very long that although many electrons have reached the surface of the insulator, hardly any electrons have enough time to diffuse. Consequently, the surface potential increases just by concentrating on the central surface's small zone. When time t = 30 s, it is obvious to see not only a sharp reduction but also an increment in the center of the surface potential. It's because an increasing number of surface charges have diffused with time from the central area. The surface potential gradient's decrease is even clearer when time t = 60 s but the central surface potential's growth becomes negligible.

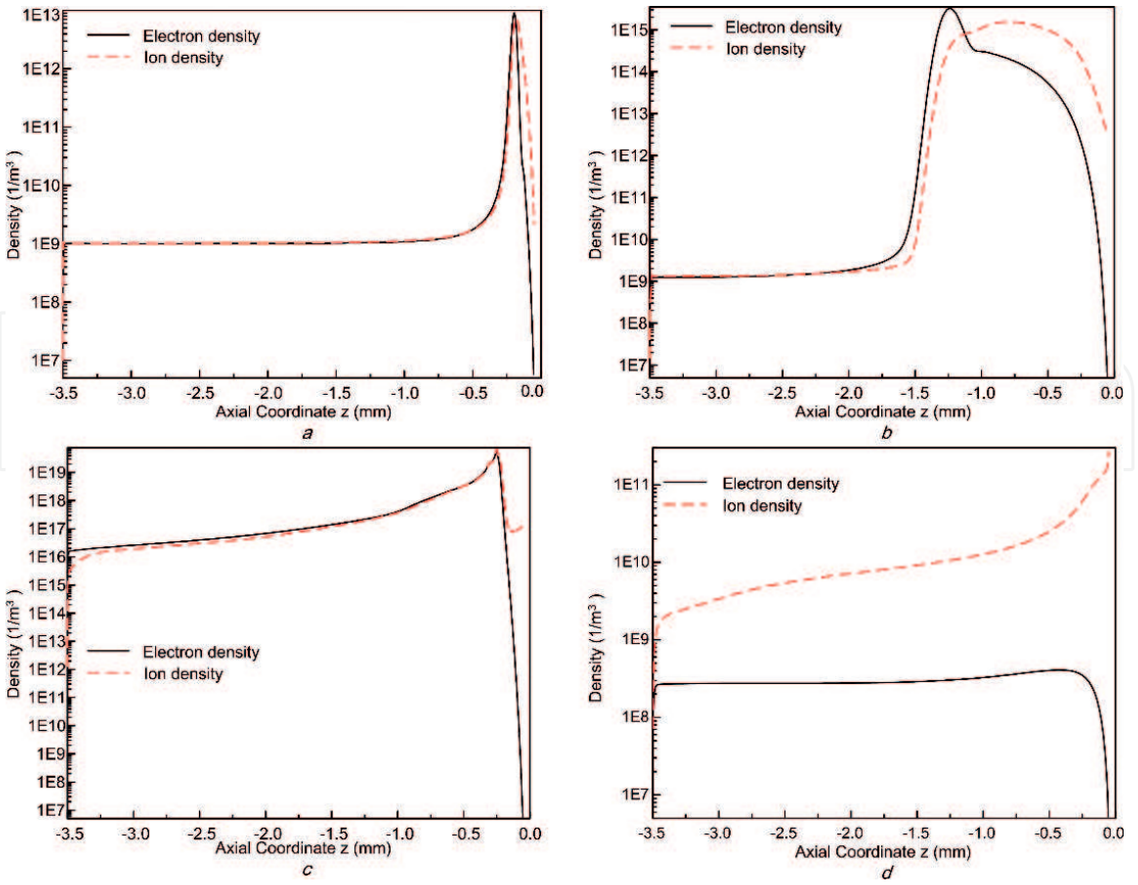

Figure 5.
The distribution of electron and ion density along the symmetry axis: (a) 1 × 10⁻⁹ s, (b) 1.8 × 10⁻⁸ s, (c) 4.6 × 10⁻⁷ s, (d) 60 s.

According to **Figure 6b**, the E-field strength distributions are shown along the symmetry axis. It's obvious that the field strength's sharp decrease occurs at the interface of insulator and air because of the epoxy insulator's higher relative dielectric constant compared with that of air. With the development of the corona discharge, an increasing number of electrons will exist on the insulator surface. The inside E-field strength's increment in insulator is caused by higher surface potential. The E-field strength at needle tip decreases as time goes by due to the decrease of the potential difference between the insulator surface and the needle tip. The E-field strength at needle tip is presented in **Figure 6b**'s margin for the purpose of seeing the outcome obviously.

When the epoxy insulator is injected with electrons, they tend to transport to GND electrode across the bulk under the built-in electric area. Several mobile electrons are possible to be captures by traps at the time of transporting and later on gain de-trapped by thermal excitation. Owing to the exceeding existence and low mobility of trapped electrons, the injected electrons are able to be observed just in insulator's skin layer. According to **Figure 7**, the distribution of trapped electrons and the mobile along symmetry axis is shown from GND electrode to insular upper surface. d = 0.5 mm is GND electrode while d = 0 mm is epoxy insulator's upper surface. According to **Figure 7a**, it is quite obvious to see that mobile electron density decreases quickly from upper surface to ground. Mobile electron increases a bit deeper in the skin layer and decreases at the upper surface. **Figure 6a** concludes that the surface potential's quick rise occurs at the beginning 1 s. In other words, most of the electrons will not be injected into epoxy insulator within the rest 59 s. Nevertheless, many electrons have gone deeper in skin layer under electric force. Consequently, electron density reduces at upper surface as time goes by. According

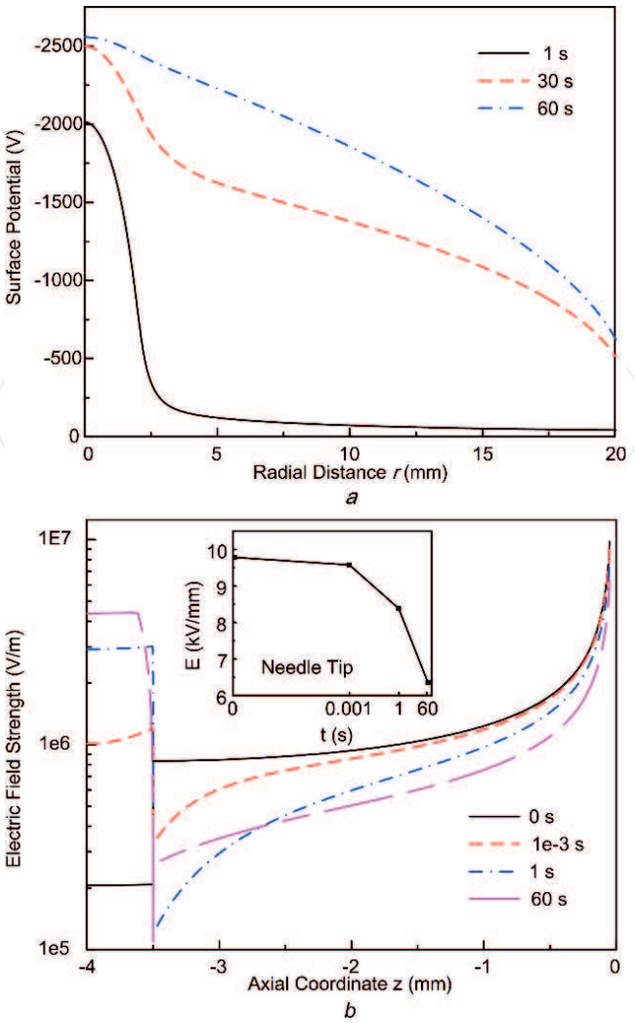

Figure 6.
The surface potential and electric field distributions: (a) surface potential and (b) electric field.

to **Figure 7b**, the trapped electrons' density increases obviously with time in the skin layer because an increasing number of mobile electrons get trapped but seldom escape at the time of transporting to the ground.

According to **Figure 8**, the central surface potential grows with time when various kinds of charging voltages are applied. It is clear central surface potential's absolute value goes up quickly. The surface potential increases sharply at the beginning 1 s under −5 kV. Later on, the growth gradually slows down with time. At last, the surface potential may reach saturation with the dissipation procedure in dynamic equilibrium and the surface charge accumulation when there is enough discharge time. When the charging voltage reduces, the surface potential in the center will spend more time to reach saturation.

According to **Figure 9**, the comparison between experimental and computational surface potential distributions is presented under −5 kV. The difference is very clear between the outcomes of the simulation and the experiment resources when t = 30 s which is presented in **Figure 9a**. The simulated value is higher than the experimental surface potential at the center. However, the experimental potential will become much higher within the area around ∼ 15 mm away from the center. Firstly, it is possible that the probe's precision will not be high enough. Secondly, several seconds were taken to take off the power source and move the insulator before measuring its surface potential. Many accumulated electrons have spread in the surrounding areas from the center in the time delay, which increases the surface potential in the surrounding regions but decreases the surface potential at the

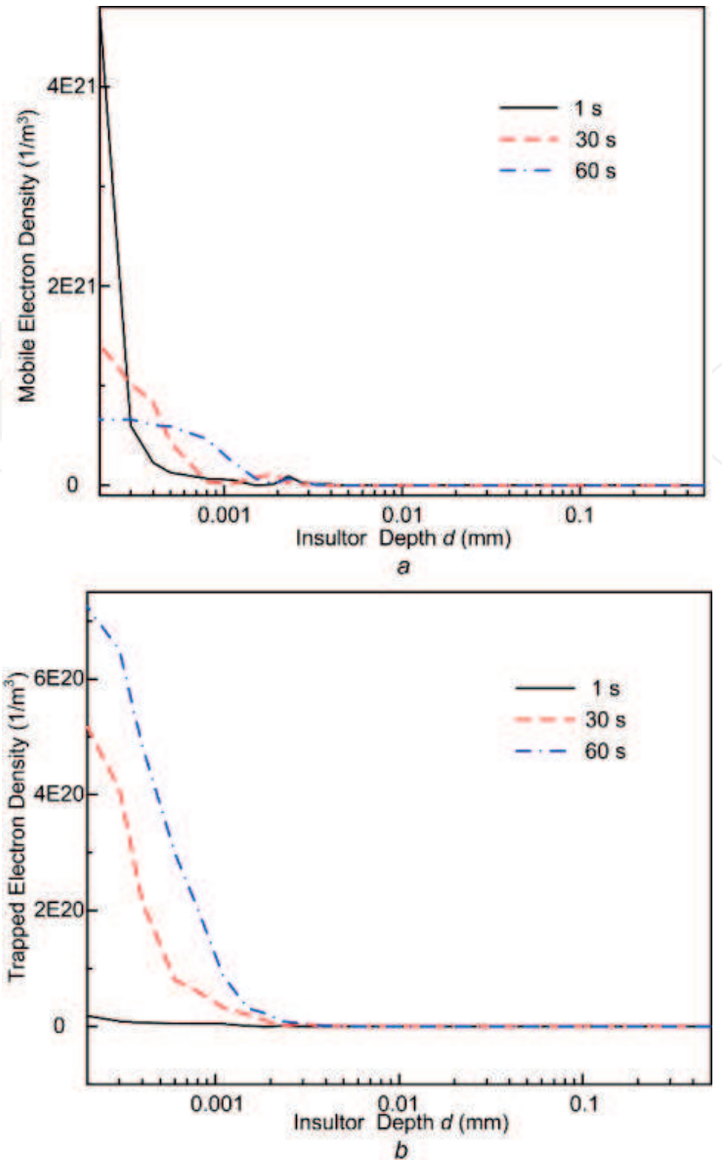

Figure 7.
The mobile and trapped electron density distribution along the symmetry axis of insulator bulk: (a) mobile electron and (b) trapped electron.

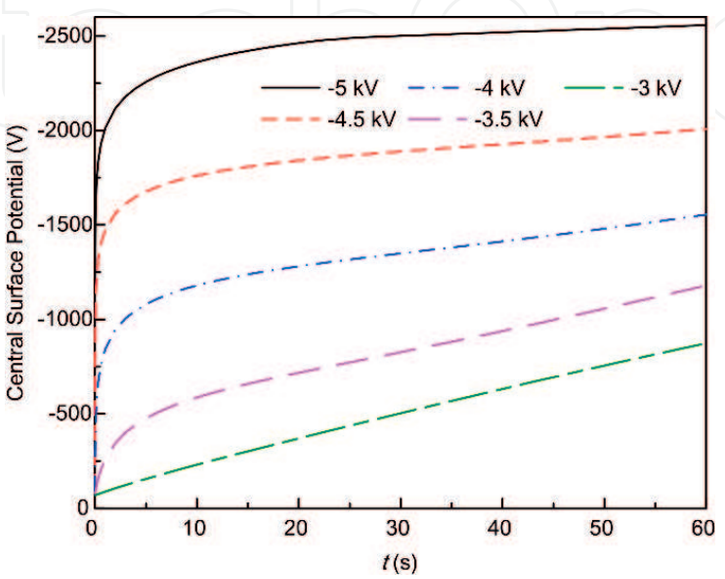

Figure 8.
The growth of central surface potential with time under different charging voltages.

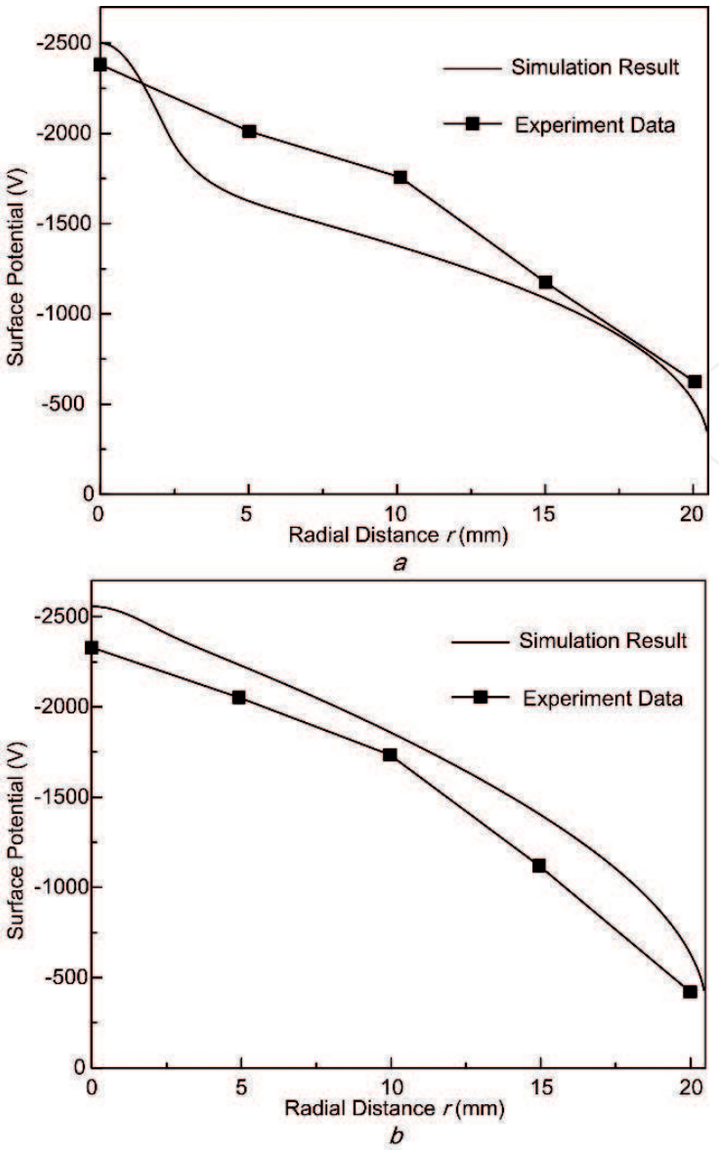

Figure 9.
The comparison between the computational and experimental surface potential distributions: (a) t = 30 s, (b) t = 60 s.

center. According to **Figure 9b**, two similar curves of experimental and computational surface potential distributions are shown when t = 60 s. nevertheless, it is evident that the simulated values are higher than the experimental resources. The time delay is possible to be responsible before the surface potential measurement.

According to **Figure 10**, epoxy insulator's central surface potentials are presented under various kinds of voltages after the charging for 60 s. It is obvious to see both the simulated and measured potential values grow up nearly in a linear way with the charging voltage at the insulator center. According to **Figure 10b**, the central potential grows with time under −5 kV. Experimental resources present a nice agreement with the outcomes of the simulation that central potential goes up quickly at the beginning seconds and at last reaches a fixed condition. Because of the diffusion of charges from center, the outcomes of the simulation are often higher than the measured surface potentials, particularly at the beginning 10 s. According to what has been discussed in **Figure 5**, the gradient of the surface potential distribution is much clearer along the radial distance at the beginning 10 s. Therefore, the central surface charges' spread around is clearer to cause a greater effect on measured surface potential. Thus, the difference between the outcomes of the simulation and the experimental resources is wider at the beginning 10 s.

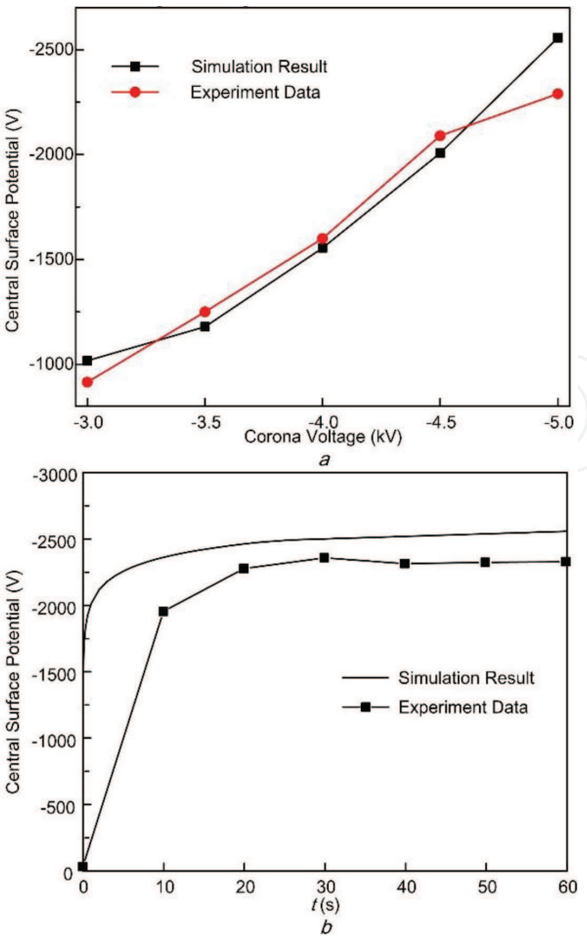

Figure 10.
The comparison between the computational and experimental central surface potentials: (a) the central surface potentials after 60s' charging and (b) the growth of central surface potential with time.

4. Conclusions

The accumulation procedure of the surface charge under the needle-plane corona discharge has been explored in This chapter and some comparisons between experimental resources and the simulation outcomes have also been made. The major conclusion is shown below:

1. In the accumulation procedure of the surface charge, the corona discharge intensity increases at the beginning and later reduces as time goes by. The epoxy insulator's surface potential has increased sharply first and later slowly reaches saturation.

2. The surface potential distributions' curves have various kinds of shapes at various periods. As time goes by, the surface potential gradient along epoxy insulator's radial distance reduces because of the surface charge's diffusion.

3. Meanwhile, a higher central surface potential exists in the epoxy insulator under higher charging voltage when it is being charged. Then, the central surface potential takes a shorter time to reach saturation.

4. The epoxy insulator's skin layer has a surface charge. These mobile electrons have a tendency to cross the insulator to the GND electrode. Among them, some get trapped and gradually get detrapped by thermal excitation.

Author details

Boxue Du, Hucheng Liang and Jin Li*
Key Laboratory of Smart Grid of Education Ministry, School of Electrical and Information Engineering, Tianjin University, Tianjin, China

*Address all correspondence to: lijin@tju.edu.cn

IntechOpen

References

[1] Kumara S, Alam S, Hoque IR, et al. DC flashover characteristics of a polymeric insulator in presence of surface charges. IEEE Transactions on Dielectrics and Electrical Insulation. 2012;**19**(3):1084-1090

[2] Kumara S, Serdyuk YV, Gubanski SM. Simulation of surface charge effect on impulse flashover characteristics of outdoor polymeric insulators. IEEE Transactions on Dielectrics and Electrical Insulation. 2010;**17**(6): 1754-1763

[3] Du BX, Li ZL. Surface charge and DC flashover characteristics of direct-fluorinated SiR/SiO_2 nanocomposites. IEEE Transactions on Dielectrics and Electrical Insulation. 2015;**21**(6): 2602-2610

[4] Nakanishi K, Yoshioka A, Arahata Y, et al. Surface charging on epoxy spacer at DC stress in compressed SF6 gas. IEEE Transactions on Power Apparatus and Systems. 1983;**102**(12):3919-3927

[5] Sato S, Zaengl WS, Knecht A. A numerical analysis of accumulated surface charge on dC epoxy resin spaces. IEEE Transactions on Electrical Insulation. 1987;**22**(3):333-340

[6] Mohamad A, Chen G, Zhang Y, et al. Mechanisms for surface potential decay on fluorinated epoxy in high voltage DC applications. IEEE Conference on Electrical Insulation and Dielectric Phenomena (CEIDP). 2014. pp. 863-866

[7] Du BX, Zhang JW, Gao Y. Effect of nanosecond rise time of pulse voltage on the surface charge of epoxy/TiO_2 nanocomposites. IEEE Transactions on Dielectrics and Electrical Insulation. 2013;**20**(20):321-328

[8] Roy SL, Segur P, Teyssedre G, Laurent C. Description of bipolar charge transport in polyethylene using a fluid model with a constant mobility: Model prediction. Journal of Physics D: Applied Physics. 2003;**37**(2):298

[9] Min D, Li S. Simulation on the influence of bipolar charge injection and trapping on surface potential decay of polyethylene. IEEE Transactions on Dielectrics and Electrical Insulation. 2014;**21**(4):1627-1636

[10] Chen G. A new model for surface potential decay of corona-charged polymers. Journal of Applied Physics. 2010;**43**(5):55405-55411

[11] Zhou F, Li J, Yan Z, et al. Investigation of charge trapping and detrapping dynamics in LDPE, HDPE and XLPE. IEEE Transactions on Dielectrics and Electrical Insulation. 2017;**23**(6):3742-3751

[12] Min D, Li S, Li G. The effect of charge recombination on surface potential decay crossover characteristics of LDPE. IEEE International Symposium on Electrical Insulating Materials (ISEIM). 2014. pp. 104-107

[13] He W, Liu XH, Yang F, et al. Numerical simulation of direct current glow discharge in air with experimental validation. Journal of Applied Physics. 2012;**51**(51):6001

[14] Nahomy J, Ferreira CM, Gordiets B, et al. Experimental and theoretical investigation of a N_2-O_2 DC flowing glow discharge. Journal of Physics D. 1995;**28**(4):738

[15] Choi J, Matsuo K, Yoshida H, et al. Characteristics of a DC-driven atmospheric pressure air microplasma jet. Journal of Applied Physics. 2008; **47**(8):6459-6463

[16] Tochikubo F, Arai H. Numerical simulation of streamer propagation and

radical reactions in positive corona discharge in N_2/NO and N_2/O_2/NO. Journal of Applied Physics. 2002;**41** (2A):844-852

[17] Itikawa Y, Ichimura A. Cross sections for collisions of electrons and photons with atomic oxygen. Journal of Physical and Chemical Reference Data. 1990;**19**(3):637-651

[18] Itikawa Y. Cross sections for electron collisions with nitrogen molecules. Journal of Physical and Chemical Reference Data. 2006;**34**(38): 1-20

[19] Zhou T, Chen G, Liao R, Xu Z. Charge trapping and detrapping in polymeric materials: Trapping parameters. Journal of Applied Physics. 2009;**106**(12):644-637

[20] Chen G, Zhao J, Zhuang Y. Numerical modeling of surface potential decay of corona charged polymeric material. IEEE International Conference Solid Dielectrics (ICSD). 2010. pp. 1-4